Materials Science in Semiconductor Processing 198 (2025) 109797

Contents lists available at ScienceDirect

Materials Science in Semiconductor Processing

journal homepage: www.elsevier.com/locate/mssp

High on/off ratio ZnS-based ReRAM with multi-level switching characteristics

Sang-Hun Lee [a,b], Sobia Ali Khan [a], Sung-Min Hong [b], Jae-Hyung Jang [a,c,*]

[a] KENTECH Institute of Energy Materials and Devices, KENTECH, Naju, 58330, South Korea
[b] School of Electrical Engineering and Computer Science, Gwangju Institute of Science and Technology, Gwangju, 61005, South Korea
[c] Department of Energy Engineering, Korea Institute of Energy Technology, Naju, 58330, South Korea

ARTICLE INFO

Keywords:
Resistive random-access memory
ZnS
On/off ratio
Multi-level switching

ABSTRACT

Resistive random-access memory (ReRAM) devices based on zinc sulfide (ZnS) were fabricated and characterized. The devices consist of a Ti/Pt bottom electrode (BE), radio-frequency magnetron sputtered 30-nm-thick ZnS switching layer, and a 150-nm-thick Ag top electrode (TE). X-ray photoelectron spectroscopy (XPS) confirmed the chemical composition and identified intrinsic defects in ZnS, contributing to the resistive switching. Electrical measurements reveal stable cycling behavior, high on/off ratio ($\sim 5 \times 10^3$), excellent endurance ($\sim 2 \times 10^3$ cycles), and good retention ($\sim 6 \times 10^3$ s) characteristics. Cycle-to-cycle and device-to-device variability analysis demonstrated low coefficients of variation (CVs) for resistance states and switching voltages, suggesting stable operation and high uniformity. The resistive switching is attributed to conductive filament (CF) formation and rupture driven by Ag ion migration through ZnS bulk defects. Multi-level switching was achieved by controlling the writing current (I_W) and evaluated using bit error rate (BER) analysis. The ZnS-based ReRAM exhibited reliable multi-level switching characteristics up to six distinct resistance states, indicating its potential for high-density memory devices.

1. Introduction

Resistive random access memory (ReRAM) has emerged as one of the highly promising candidates for the future non-volatile memory devices because it offers various advantages such as high speed read and write [1–4], high scalability [3,4], low power consumption [1–3], compatibility with silicon electronics technology [1,2], and multi-level information storage capabilities [4].

ReRAMs typically adopt metal-insulator-metal (MIM) structures, with various materials such as oxides [5–8], chalcogenides [9–12], and organic materials [13,14] utilized in the resistive switching layer. To evaluate the performance of ReRAM devices, critical parameters such as endurance, retention, on/off ratio, and device uniformity were considered. The on/off ratio ensures a clear distinction between the high resistance state (HRS) and low resistance state (LRS), enabling reliable data storage and retrieval. Thus, high on/off ratio is essential for minimizing read errors and improving data integrity, contributing significantly to the overall efficiency and reliability of the device [15,16]. In addition, the ability to perform multi-level switching has emerged as a crucial performance metric for next-generation ReRAM devices. Multi-level switching not only enhances the capacity and spatial efficiency of memory devices [4,17] but also plays a vital role in achieving the requirements of neuromorphic computing [18,19], a rapidly growing field of ReRAM.

ZnS, a wide-bandgap (3.72–3.77 eV) sulfide-based chalcogenide material, offers notable advantages, including optical transparency in the visible and infrared spectral range, chemical stability, and mechanical durability. Despite these promising properties, its application in the ReRAM field has been limited. Prior studies have primarily utilized ZnS in hybrid structures—such as ZnS–SiO_2 composites [20], Ag-nanocluster-embedded ZnS [21] or as a shell layer in core–shell quantum dots (e.g., CdSe/ZnS, InP/ZnSe/ZnS) [22–24]. Consequently, the key performance parameters like retention, endurance, and multi-level switching behavior and the conductive and switching mechanisms in pure ZnS-based systems have not been thoroughly investigated, and the underlying switching mechanisms remain poorly understood.

This study addresses these gaps by exploring the performance of ZnS-based ReRAM devices. In this work, we demonstrate that a single-layer ZnS thin film, deposited between Ag and Pt electrodes, exhibits reliable

* Corresponding author. KENTECH Institute of Energy Materials and Devices, KENTECH, Naju, 58330, South Korea
E-mail address: jjang@kentech.ac.kr (J.-H. Jang).

https://doi.org/10.1016/j.mssp.2025.109797
Received 27 March 2025; Received in revised form 16 May 2025; Accepted 17 June 2025
Available online 19 June 2025

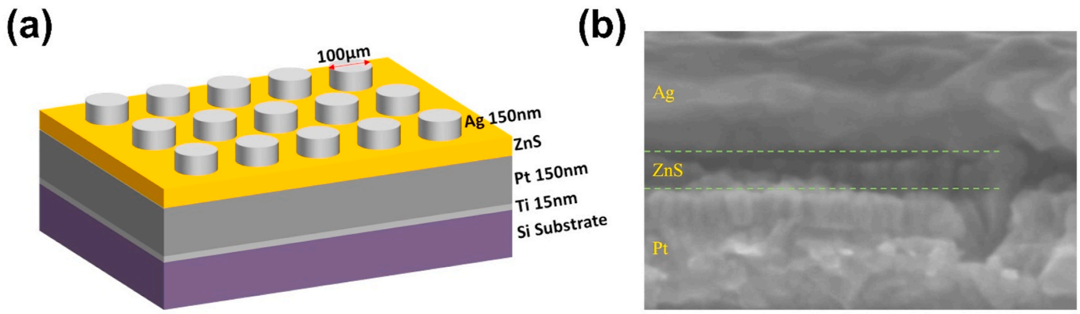

Fig. 1. (a) Schematic structure and (b) cross section image of the ZnS-based ReRAM.

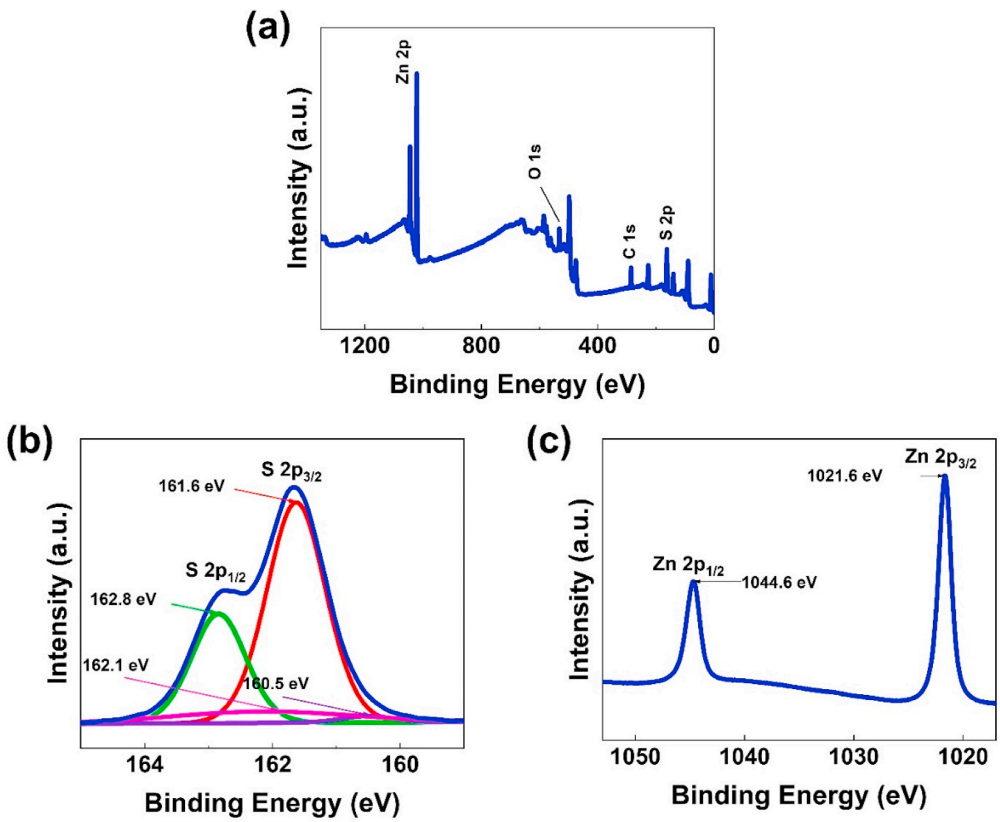

Fig. 2. XPS spectra of ZnS: (a) survey of spectrum, (b) Zn2p, and (c) S2p.

bipolar switching without requiring any additional hybridization or nanostructuring. The ZnS-based ReRAM device exhibits a high on/off ratio exceeding 5×10^3, stable endurance up to 2×10^3 cycles, and retention beyond 6×10^3 s. More importantly, it supports six statistically distinguishable resistance states, achieved by tuning the writing current (I_W) during the SET process. The distinctiveness of these states is quantitatively verified using bit error rate (BER) analysis, with all adjacent states exhibiting BER values below 4 %, thereby confirming their stability and reproducibility. Despite the relatively unexplored use of ZnS in ReRAM, the electrical performance demonstrated here rivals or surpasses that of many conventional oxide- and sulfide-based ReRAM devicess. These findings position ZnS as a promising candidate for high-density multi-level memory and neuromorphic computing applications.

2. Experiments

The device fabrication process involved depositing a Ti/Pt (15/150 nm) bottom electrode (BE) onto a Si substrate using e-beam evaporation. The 30-nm-thick ZnS films were then deposited at room temperature using radio frequency (RF) magnetron sputtering under an argon gas flow rate of 55 SCCM, pressure of 20 mTorr, and dc power of 60 W. X-ray photoelectron spectroscopy (XPS) was utilized to analyze the chemical composition of the deposited ZnS. A 150-nm-thick Ag top electrode (TE) was deposited using an electron beam evaporation method. A schematic diagram of the fabricated devices is shown in Fig. 1a and field emission scanning electron microscopy (FE-SEM) cross sectional image of Ag-ZnS-Pt structure is shown in Fig. 1b. The FE-SEM work at Korea Institute of Energy Technology (KENTECH) was supported by Center for Shared Research Facilities. The electrical characteristics were measured at room temperature and atmospheric pressure by using a Keithley 4200-SCS semiconductor parameter analyzer. The bias voltage was applied to the TE while the BE was grounded.

3. Results and discussion

XPS was utilized to analyze the chemical composition of the

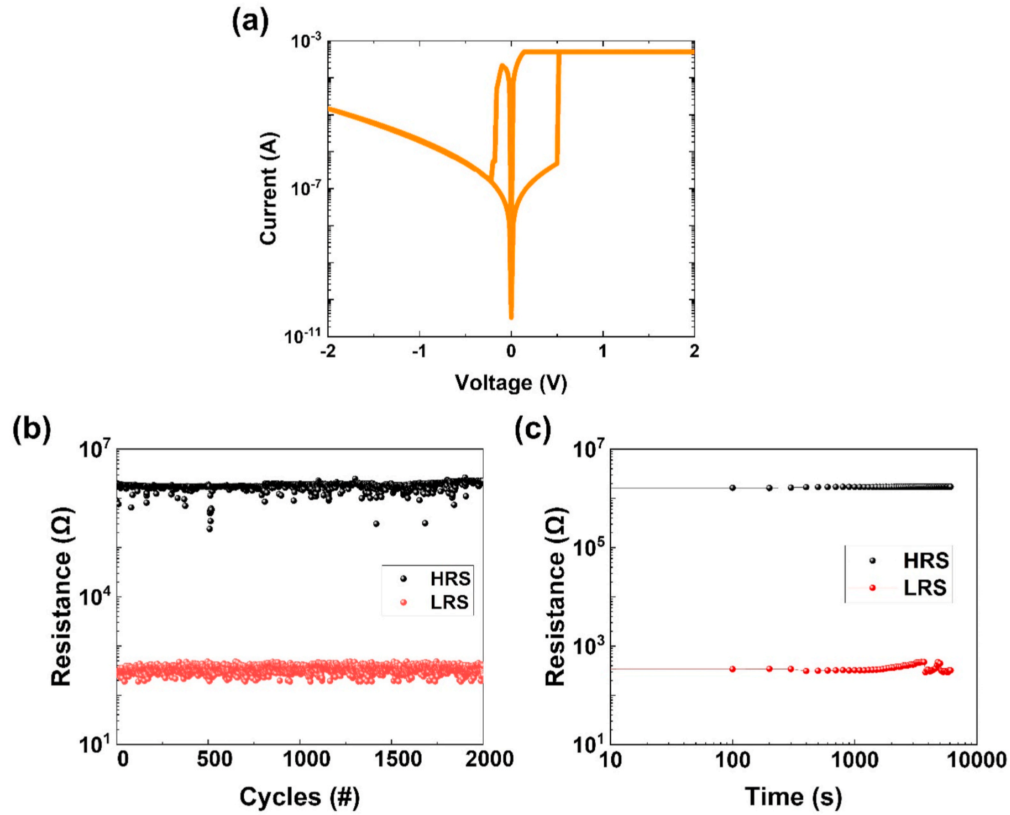

Fig. 3. Electrical characteristics of the ZnS-based ReRAM: (a) typical I-V curve, (b) endurance up to 2×10^3 cycles, and (c) retention up to 6×10^3 s.

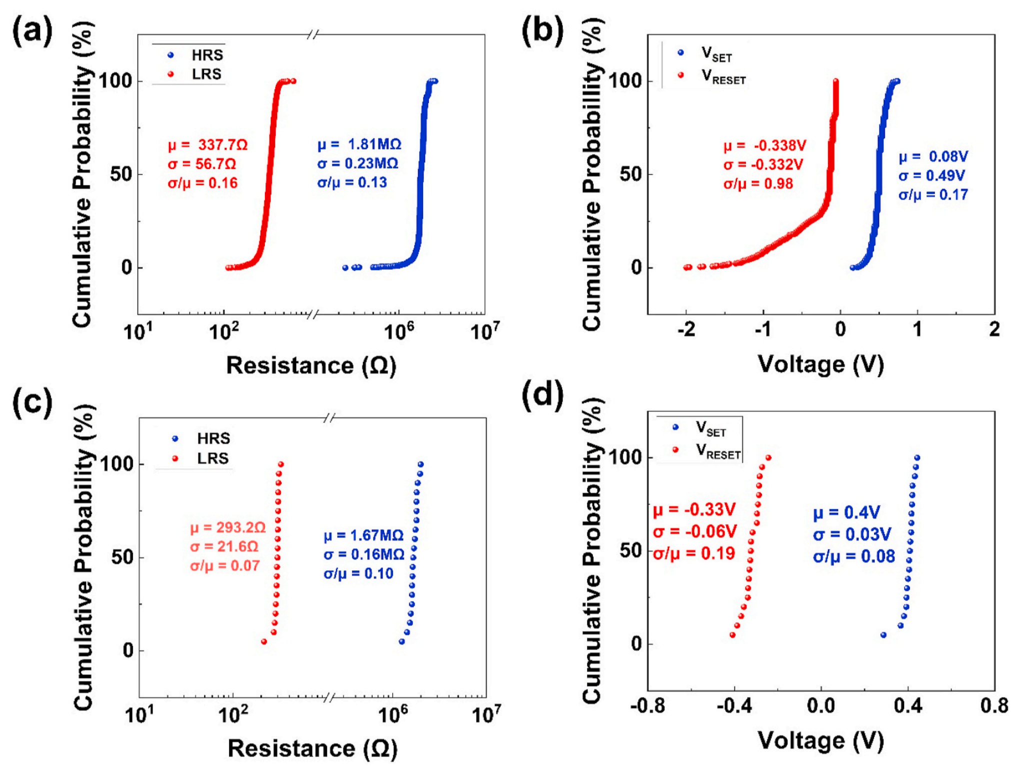

Fig. 4. (a) Cycle-to-cycle cumulative probability of HRS and LRS, and (b) V_{SET} and V_{RESET}. (c) Device-to-device cumulative probability of HRS and LRS, and (d) V_{SET} and V_{RESET}, where μ is average and σ is standard deviation.

Table 1
Comparison of on/off ratio, $\mu(V_{SET})$, and $\mu(V_{RESET})$ of reported ReRAMs.

Device Structure	On/off ratio	$\mu(V_{SET})$	$\mu(V_{RESET})$	Ref.
Ag/ZnS/Pt	~5 × 10^3	0.49V	−0.34V	This work
Ag/WS_2/Pt	400	3.12V	−2.93V	[22]
Ag/MoS_2/Pt	40	0.8V	−0.6V	[12]
Ag/CoS_x/Co	< 10^3	−1.10V	0.32V	[14]
W/MoO_x/MoS_xO_y/FTO	~200	1.06V	−2.36V	[30]
Cu/BN/SiO_2/Pt	60–80	~1.3V	-2V	[31]
Au/Gd_2O_3/TiN	10	1V	-2V	[32]
Al/TaO_x/Pt	10^3	2V	-2V	[33]
TiW/ZnS-SiO_2/Cu	~10^2	~0.6V	~-0.2V	[20]
Ag/ZnS-Ag/ZnS/ITO	~5 × 10^3	0.3V	−0.15V	[21]
Al/InP-ZnSe-ZnS QDs/ITO	16.6	0.73V	-2V	[22]
Al/PMMA/InP-ZnSe-ZnS QDs/ ITO	35.5	1.06V	-2V	[22]
Ag/ZnSe-ZnS QDs/ITO	~5 × 10^3	0.57V	−1.02V	[23]

deposited ZnS. Distinct peaks for Zn2p, O1s, C1s, and S2p are observed as shown in Fig. 2a, which align with the typical ZnS XPS spectra [25]. In Fig. 2b, the Zn2p peak is deconvoluted into a $Zn2p_{1/2}$ peak (1044.6 eV) and a $Zn2p_{3/2}$ peak (1021.6 eV). The energy difference between these two peaks is approximately 23 eV, which is typical for Zn^{2+} ions in ZnS, indicating the chemical state of Zn in ZnS [26]. Similarly, Fig. 2c shows $S2p_{1/2}$ and $S2p_{3/2}$ peaks at 162.8 and 161.6 eV, respectively, indicating the presence of sulfide (S^{2-}) ions [27]. Additionally, relatively small peaks, observed at 160.5 and 162.1 eV, which are attributed to the presence of defects within the ZnS [28], which can influence in formation and rupture of conductive filaments. These defects serve as a migration site for Ag ions. The migration of Ag ions through these defects forms conductive filament, which play an important role in the state transitions of HRS and LRS in ReRAM.

The electrical characteristics of the ReRAM with 30-nm-thick ZnS are shown in Fig. 3. Fig. 3a illustrates the typical cycling behavior of the fabricated ZnS-based ReRAM. To prevent permanent breakdown during the SET process, the compliance current was set to be 500 μA. Fig. 3b shows the endurance characteristics up to 2 × 10^3 cycles, which were measured at read voltage of 0.02 V. Devices exhibit stable operation during cycles, with an on/off ratio of 5 × 10^3. Fig. 3c shows the retention characteristics at room temperature. Both high resistance state (HRS) and low resistance state (LRS) were maintained for 6 × 10^3 s. These performances demonstrate that ZnS-based ReRAM devices are promising candidates for resistive switching memory devices.

To evaluate the uniformity of the ZnS-based ReRAM devices, the cycle-to-cycle and device-to-device variability of the HRS, LRS, V_{SET}, and V_{RESET} were analyzed using cumulative probabilities. Cycle-to-cycle variability is illustrated in Fig. 4a and b. Statistical analysis shows that the coefficients of variation (CVs) for LRS, HRS, V_{SET}, and V_{RESET} are 0.16, 0.13, 0.17 and 0.98, respectively. The consistently low CVs of all four indicators [29] suggest low cycle-to-cycle variability, confirming the stable operation of the devices within the ±2 V range. To evaluate the device-to-device variability, CVs of LRS, HRS, V_{SET}, and V_{RESET} are also calculated, and they are found to be 0.07, 0.1, 0.08, and 0.19, respectively, as shown in Fig. 4c and d. It also shows low CVs, which indicates high uniformity between ZnS-based ReRAMs. Table 1 compares the on/off ratios and average switching voltages between sulfide-based ReRAMs with a TE consisting of Ag and recently reported ReRAMs. The proposed single-layer ZnS-based ReRAM exhibits a significantly higher on/off ratio approximately five times greater than other sulfide-based devices and lower switching voltages compared to both sulfide- and oxide-based ReRAMs. In addition, its shows competitive performance compared to previously reported ZnS composites or quantum dot ReRAMs. These results demonstrate that, even without

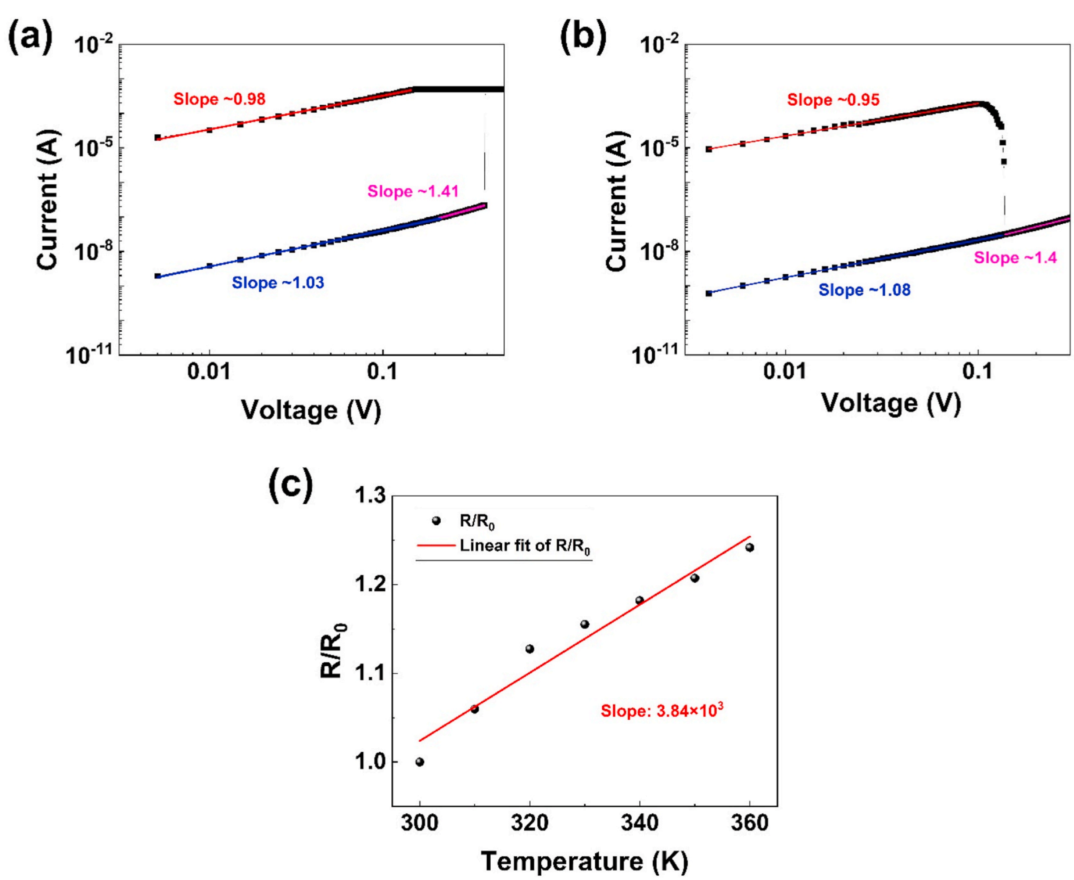

Fig. 5. Log(V)-Log(I) plot of (a) SET process and (b) RESET process. (c) Temperature – Resistance plot in LRS.

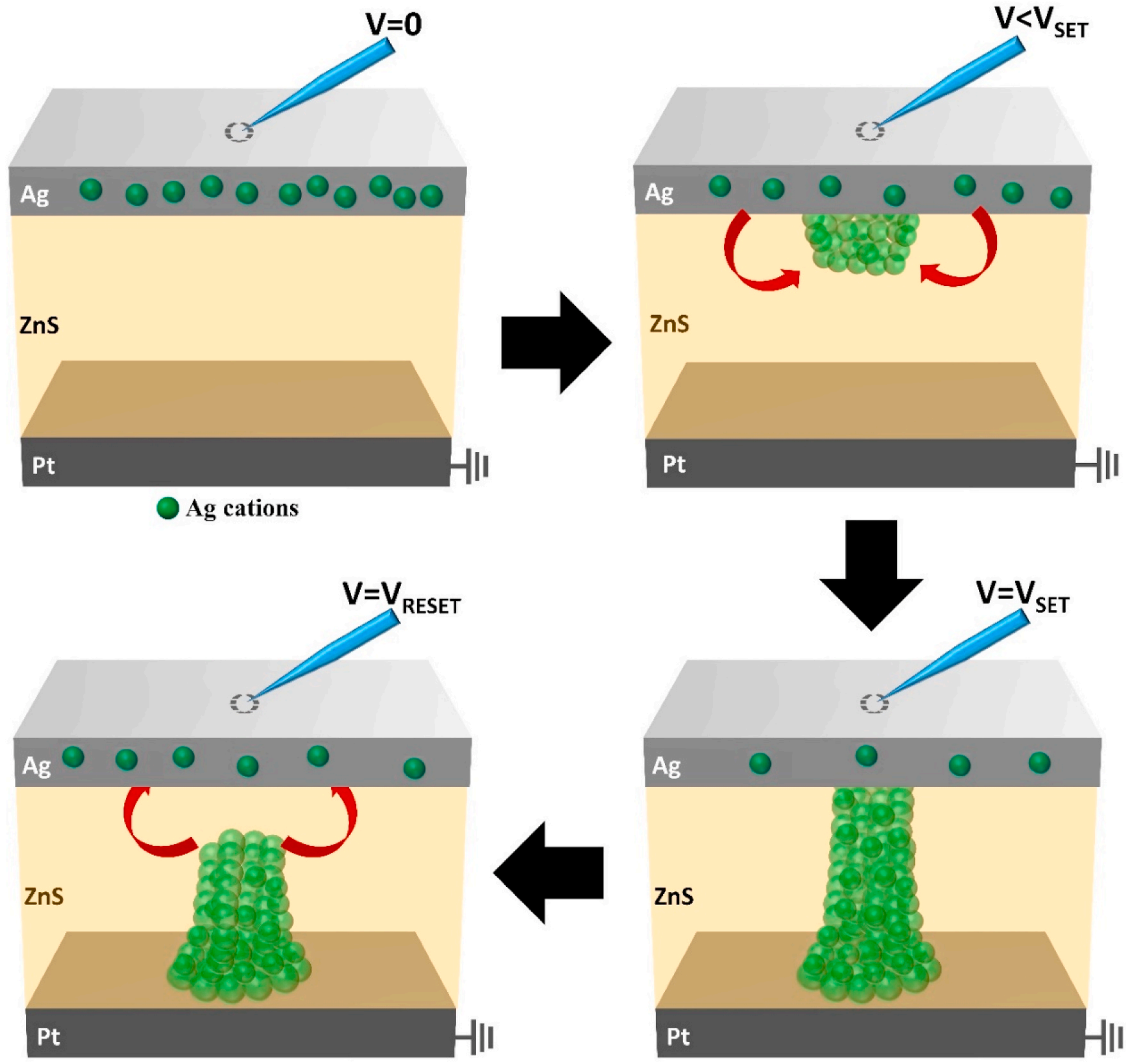

Fig. 6. Schematics of the switching mechanism of ZnS-based ReRAM.

hybridization or composite structures, single-layer ZnS can deliver competitive performance, underscoring its potential as an alternative material for high-performance ReRAM applications.

To investigate the conduction mechanism of ZnS-based ReRAM, the space-charge-limited current (SCLC) model was applied. Fig. 6a and b shows Log(V) –Log (I) plot of SET and RESET process. In the HRS low voltage region during the SET process, the slope of the I-V curve is approximately 1, indicating that this region follows ohmic conduction. In this region, the number of injected carriers is smaller than that of the thermally generated carriers, and the current follows the ohmic conduction behavior. As the voltage increases to a region with a slope of approximately 1.4, the number of injected carriers exceeds that of the thermally generated carriers, but they are still insufficient to fill all the traps in ZnS switching layer. This region is referred to as the trap-limited SCLC region. At the V_{SET}, the current suddenly increases, indicating that the injected carriers have filled all the traps in the material. At this point, the current no longer depends on traps, and this rapid increase in current is called trap-filled limited conduction, which transitions the device from HRS to LRS. In the low voltage region of LRS, the behavior of the device returns to ohmic conduction, similar to the LRS ohmic conduction region [34,35]. In the RESET process, current exhibits a similar conduction behavior. These results suggest that the conduction mechanism of ZnS-based ReRAM is governed by ohmic conduction in the lower voltages and trap-limited SCLC in the higher voltages for both SET and RESET states, demonstrating a consistent conduction behavior throughout the switching process. According to these behaviors in the LRS and HRS, the conduction mechanisms of the ZnS-based ReRAM are similar with those of the other sulfide-based ReRAM devices with Ag CFs [9,11,36]. To verify the Ag CFs involved in the conduction mechanism, the resistance change with temperature in the low resistance state (LRS) was analyzed using the following equation:

$$R(T) = R_0[1 + \alpha(T - T_0)] \quad [1]$$

Where R_0 is the resistance at the temperature, T_0, and α is the temperature coefficient. Fig. 5c shows the experimental data and the corresponding linearly fitted curve plotted on the R/R_0 versus temperature (T) graph. It shows a slope of approximately 3.84×10^{-3} K^{-1}, which closely matches the positive temperature coefficient of Ag [37–40]. This suggests that Ag conductive filaments are formed during the operation of the ZnS-based ReRAM. These findings confirm the migration of Ag cations leads to the formation of conductive paths within the ZnS switching layer, thereby contributing to the resistive switching mechanism.

Fig. 6 illustrates the switching mechanism of the ZnS-based ReRAM, as determined based on the conduction mechanism discussed above and the XPS data. Initially, in the absence of applied voltage, defects are observed within the bulk of ZnS, as indicated by the XPS analysis. Upon the application of positive bias to the TE, Ag oxidation occurs,

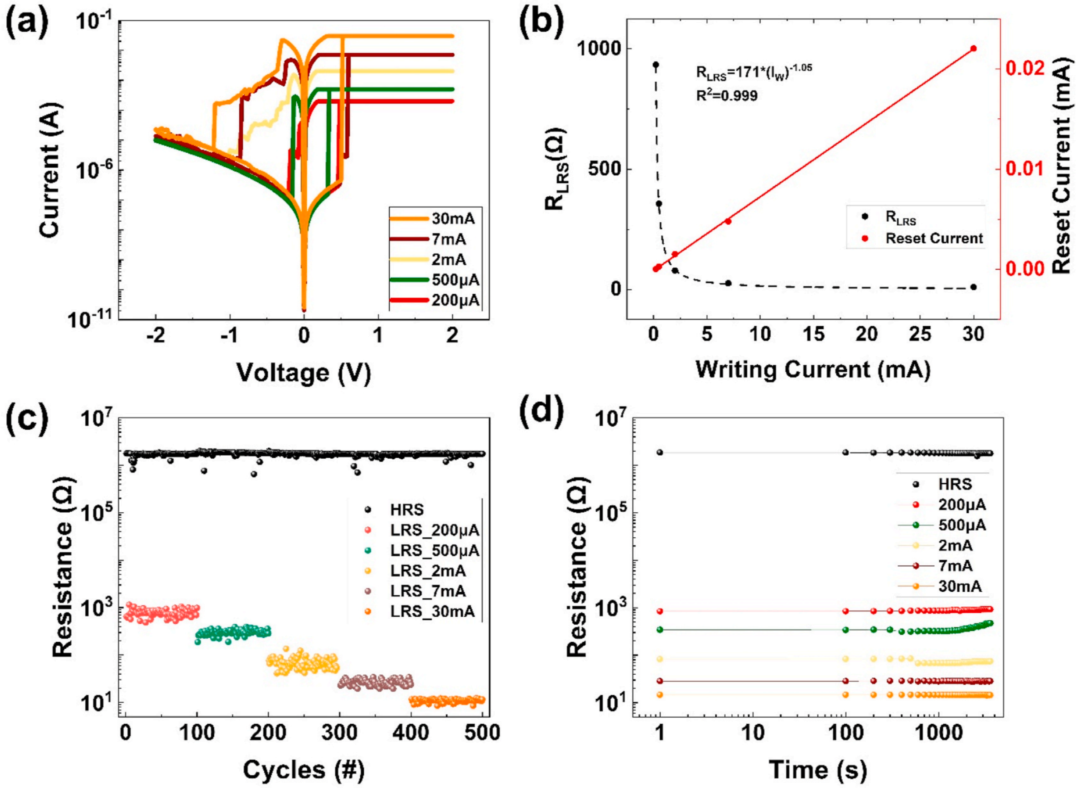

Fig. 7. Multi-level switching characteristics of ZnS-based ReRAM: (a) I-V curves for the five different writing currents (I_W), (b) relationship between the LRS and the reset current according to I_W, (c) endurance characteristics of the six distinct resistance states for 100 cycles, and (d) retention characteristics of the six resistance states for 3.6×10^3.

Table 2
Mean, standard deviation, and BER of six states.

State pairs	μ_1	μ_2	σ_1	σ_2	BER (%)
$0 \leftrightarrow 1$	1.7×10^6	774.71	1.7×10^5	127.54	7.72×10^{-28}
$1 \leftrightarrow 2$	774.71	301.24	127.54	37.05	0.0182
$2 \leftrightarrow 3$	301.24	68.62	37.05	16.76	5.33×10^{-7}
$3 \leftrightarrow 4$	68.62	26.78	16.76	3.66	0.7372
$4 \leftrightarrow 5$	26.78	10.98	3.66	0.77	0.00123

generating Ag cations. These cations migrate via the defects within the bulk ZnS towards the BE, initiating the nucleation of CFs. Subsequently, when the positive bias reaches V_{SET}, CFs are formed, causing a connection between the TE and BE and leading to the resistance switching from the HRS to the LRS. To return to the HRS, a $V < V_{RESET}$ is applied to the TE, causing a reduction of Ag cations in the TE-side CFs, resulting in a rupture of the CFs.

The multi-level switching characteristics of the ZnS-based ReRAM were investigated by adjusting the writing current (I_W) [4,41]. Fig. 7a presents the I-V curves for various I_W values, revealing distinctive resistance states at 0.2, 0.5, 1.0, 7.0, and 30 mA. Fig. 7b shows the dependence of R_{LRS} and reset current (I_{RESET}) - defined as the maximum current value during the reset process - on I_W. As the I_W increases, the wider CFs are formed, allowing the higher filament current. To rupture the expanded CFs, a higher I_{RESET} is required during the reset process, which indicates that the ZnS-based ReRAM exhibits the typical multi-level switching behavior [42]. Although these resistance states were controlled by adjusting I_W, each state must be verified to be stable and distinguishable, rather than arbitrarily induced. Fig. 7c shows that each resistance state maintains stable switching over 100 cycles and Fig. 7d confirms their long-term stability, with all six states maintaining their resistance values for over 3.6×10^3 s. While these results demonstrate stable multi-level switching, in principle, an infinite number of states could be generated by continuously varying I_W. However, increasing the number of states leads to greater overlap in resistance distributions, resulting in a higher BER, which reduces the distinctiveness and reliability of each resistance state. To quantitatively evaluate the separability of the states, BER between each pair of adjacent resistance states was calculated by using the following formula:

$$BER = \frac{1}{2}\, erfc\left(\frac{|\mu_1 - \mu_2|}{\sqrt{2(\sigma_1^2 + \sigma_2^2)}}\right) \qquad [2]$$

Table 2 summarizes the mean (μ), standard deviation (σ), and BER for the six states, defined sequentially from HRS to LRS, numbered from 0 (HRS) to 6 (LRS at 30 mA). According to Table 2, BER between all adjacent states pairs is below 0.74 % Previous studies have shown that neuromorphic systems based on ReRAM can tolerate error probability up to 4 % [43,44]. Therefore, six states defined in this work are statistically distinguishable for muli-level operation.

Based on these results, a resistance state is considered distinct if it meets three criteria: BER below 4 %, endurance exceeding 100 cycles, and retention longer than 3.6×10^3 s. According to Table 2, Fig. 7c and d, six distinct states can be identified, comprising one HRS and five LRS's, each corresponding to a specific I_W level. These findings confirm that the resistance states generated by adjusting I_W are electrically controllable and reproducible. The combination of low BER, high endurance, and long retention time demonstrates that the proposed ZnS-based ReRAM is suitable for reliable multi-level switching applications.

4. Conclusion

The ReRAM devices based on 30-nm-thick ZnS were fabricated and characterized, demonstrating an on/off ratio higher than 5×10^3, stable endurance and retention for 2×10^3 cycles and 6×10^3 s, respectively.

The devices exhibited consistent and stable operation with low variability in resistance states and switching voltages. Ohmic conduction was the dominant conduction mechanism in the LRS, while the HRS followed a combination of ohmic and SCLC mechanisms. The resistive switching behavior was attributed to Ag CF formation, as supported by the observed defect states in ZnS and the corresponding conduction mechanisms. Multi-level switching capability, enabling six distinct resistance states, was achieved by adjusting the I_W. These findings highlight the potential of ZnS-based ReRAM for high-density, next-generation memory technologies.

CRediT authorship contribution statement

Sang-Hun Lee: Writing – review & editing, Writing – original draft, Investigation, Formal analysis, Data curation, Conceptualization. **Sobia Ali Khan:** Conceptualization. **Sung-Min Hong:** Writing – review & editing. **Jae-Hyung Jang:** Writing – review & editing, Funding acquisition, Conceptualization.

Declaration of competing interest

The authors declare that they have no known competing financial interests or personal relationships that could have appeared to influence the work reported in this paper.

Acknowledgments

This research was supported by 'Regional Innovation Mega Project' program through the Korea Innovation Foundation funded by Ministry of Science and ICT.(Project Number: 2023-DD-UP-0015).

Data availability

Data will be made available on request.

References

[1] D. Ielmini, Resistive switching memories based on metal oxides: mechanisms, reliability and scaling, Semicond. Sci. Technol. 31 (6) (2016) 063002.
[2] H. Ryu, S. Kim, Self-rectifying resistive switching and short-term memory characteristics in Pt/HfO2/TaO x/TiN artificial synaptic device, Nanomaterials 10 (11) (2020) 2159.
[3] S. Wang, et al., Metal nanoparticles layer boosted resistive switching property in NiFe2O4-based memory devices, J. Alloys Compd. 908 (2022) 164569.
[4] F. Zahoor, T.Z. Azni Zulkifli, F.A. Khanday, Resistive random access memory (RRAM): an overview of materials, switching mechanism, performance, multilevel cell (MLC) storage, modeling, and applications, Nanoscale Res. Lett. 15 (2020) 1–26.
[5] A. Regoutz, et al., Role and optimization of the active oxide layer in TiO2-based RRAM, Adv. Funct. Mater. 26 (4) (2016) 507–513.
[6] A. Fantini, et al., Intrinsic switching behavior in HfO2 RRAM by fast electrical measurements on novel 2R test structures, in: 2012 4th IEEE International Memory Workshop, IEEE, 2012.
[7] S.-Y. Wang, et al., Improved resistive switching properties of Ti/ZrO2/Pt memory devices for RRAM application, Microelectron. Eng. 88 (7) (2011) 1628–1632.
[8] A. Prakash, D. Jana, S. Maikap, TaO x-based resistive switching memories: prospective and challenges, Nanoscale Res. Lett. 8 (2013) 1–17.
[9] L. Liu, et al., Robust resistive switching in MoS2-based memristor with Ti top electrode, Appl. Surf. Sci. 605 (2022) 154698.
[10] U. Das, et al., Uniform, large-scale growth of WS2 nanodomains via CVD technique for stable non-volatile RRAM application, Mater. Sci. Semicond. Process. 107 (2020) 104837.
[11] S. Jou, et al., Cobalt sulfide films by sulfurizing cobalt for resistive switching memory, Jpn. J. Appl. Phys. 63 (2) (2023), 02SP19.
[12] J. Jang, et al., Resistance switching characteristics of solid electrolyte chalcogenide Ag2Se nanoparticles for flexible nonvolatile memory applications, Adv. Mater. 24 (26) (2012) 3573–3576.
[13] B. Mu, et al., Organic small molecule-based RRAM for data storage and neuromorphic computing, J. Mater. Chem. C 8 (37) (2020) 12714–12738.
[14] M.K. Rahmani, et al., Fully solution-processed organic RRAM device with highly stable butterfly-shaped hysteresis, Mater. Sci. Eng., B 282 (2022) 115784.
[15] N. Wei, et al., HfOx/Ge RRAM with high ON/OFF ratio and good endurance, Electronics 11 (22) (2022) 3820.
[16] A. Gutsche, et al., Exploring area-dependent Pr0. 7Ca0. 3MnO3-based memristive devices as synapses in spiking and artificial neural networks, Front. Neurosci. 15 (2021) 661261.
[17] S. Swathi, S. Angappane, Low power multilevel resistive switching in titanium oxide-based RRAM devices by interface engineering, J. Sci. Adv. Mater. Devices 6 (4) (2021) 601–610.
[18] S. Liu, et al., Multilevel resistive switching memristor based on silk fibroin/graphene oxide with image reconstruction functionality, Chem. Eng. J. 471 (2023) 144678.
[19] S.H. Choi, et al., Reliable multilevel memristive neuromorphic devices based on amorphous matrix via quasi-1D filament confinement and buffer layer, Sci. Adv. 8 (3) (2022) eabj7866.
[20] J. Huang, et al., Electrochemical metallization resistive memory devices using $ \hbox {ZnS-SiO} _ {2} $ as a solid electrolyte, IEEE Electron Device Lett. 33 (1) (2011) 98–100.
[21] L. Zhang, et al., Localized resistive switching in a ZnS–Ag/ZnS double-layer memory, J. Phys. Appl. Phys. 47 (45) (2014) 455101.
[22] G.W. Baek, et al., Memristive switching mechanism in colloidal InP/ZnSe/ZnS quantum dot-based synaptic devices for neuromorphic computing, Nano Lett. 24 (19) (2024) 5855–5861.
[23] Z.-P. Wang, et al., Type-I core–shell ZnSe/ZnS quantum dot-based resistive switching for implementing algorithm, Nano Lett. 20 (7) (2020) 5562–5569.
[24] A.K. Yagati, et al., Recombinant azurin-CdSe/ZnS hybrid structures for nanoscale resistive random access memory device, Biosens. Bioelectron. 90 (2017) 23–30.
[25] Z.H. Ibupoto, et al., Hydrothermal synthesis of nanoclusters of ZnS comprised on nanowires, Nanomaterials 3 (3) (2013) 564–571.
[26] Y.-N. NuLi, Y.-Q. Chu, Q.-Z. Qin, Nanocrystalline ZnFe2 O 4 and Ag-doped ZnFe2 O 4 films used as new anode materials for Li-ion batteries, J. Electrochem. Soc. 151 (7) (2004) A1077.
[27] L. Dai, et al., Colloidal manganese-doped ZnS nanoplatelets and their optical properties, Chem. Mater. 33 (1) (2020) 275–284.
[28] X. Hao, et al., Zinc vacancy-promoted photocatalytic activity and photostability of ZnS for efficient visible-light-driven hydrogen evolution, Appl. Catal. B Environ. 221 (2018) 302–311.
[29] M. Tsigkourakos, et al., Ultra-low power multilevel switching with enhanced uniformity in forming free TiO2− x-based RRAM with embedded Pt nanocrystals, Phys. Status Solidi 214 (12) (2017) 1700570.
[30] W. Mu, et al., Multilevel resistive switching in MoOx/MoSxOy heterostructure memory, Mater. Sci. Semicond. Process. 174 (2024) 108191.
[31] H. Ranjan, et al., Self-rectifying and forming-free resistive switching with Cu/BN/SiO2/Pt bilayer device, Mater. Sci. Semicond. Process. 183 (2024) 108744.
[32] C. Sun, et al., Multi-factors induced evolution of resistive switching properties for TiN/Gd2O3/Au RRAM devices, J. Alloys Compd. 816 (2020) 152564.
[33] J.S. Zhao, et al., The effect of high resistivity AlOδ layer on low-power consumption of TaOx based resistive switching memory, Vacuum 174 (2020) 109186.
[34] P. Wang, et al., Bias tuning charge-releasing leading to negative differential resistance in amorphous gallium oxide/Nb: SrTiO3 heterostructure, Appl. Phys. Lett. 107 (26) (2015).
[35] C.-P. Kwan, et al., Space-charge limited conduction in epitaxial chromia films grown on elemental and oxide-based metallic substrates, AIP Adv. 9 (5) (2019).
[36] X. Yan, et al., Robust Ag/ZrO2/WS2/Pt memristor for neuromorphic computing, ACS Appl. Mater. Interfaces 11 (51) (2019) 48029–48038.
[37] S. Zhu, et al., In-depth physical mechanism analysis and wearable applications of HfO x-based flexible memristors, ACS Appl. Mater. Interfaces 15 (4) (2023) 5420–5431.
[38] N. He, et al., Reversible transition of volatile and nonvolatile switching in Ag–In–Zn–S quantum dot-based memristors with low power consumption for synaptic applications, ACS Appl. Nano Mater. 4 (3) (2021) 2365–2374.
[39] A. Bid, A. Bora, A. Raychaudhuri, Temperature dependence of the resistance of metallic nanowires of diameter⩾ 15 nm: applicability of Bloch-Grüneisen theorem, Phys. Rev. B Condens. Matter 74 (3) (2006) 035426.
[40] K. Wang, et al., A pure 2H-MoS2 nanosheet-based memristor with low power consumption and linear multilevel storage for artificial synapse emulator, Adv. Electronic Mater. 6 (3) (2020) 1901342.
[41] T.-H. Kim, et al., Multilevel switching memristor by compliance current adjustment for off-chip training of neuromorphic system, Chaos Solitons Fractals 153 (2021) 111587.
[42] A. Prakash, H. Hwang, Multilevel cell storage and resistance variability in resistive random access memory, Phys.Sci. Rev. 1 (6) (2016) 20160010.
[43] T. Hirtzlin, et al., Outstanding bit error tolerance of resistive RAM-based binarized neural networks, in: 2019 IEEE International Conference on Artificial Intelligence Circuits and Systems (AICAS), IEEE, 2019.
[44] J. Park, Neuromorphic computing using emerging synaptic devices: a retrospective summary and an outlook, Electronics 9 (9) (2020) 1414.